scientific reports

Check for updates

OPEN

Evolution of spin freezing transition and structural, magnetic phase diagram of $Dy_{2-x}La_xZr_2O_7$ ($0 \leq x \leq 2.0$)

Sheetal✉ & C. S. Yadav

$Dy_2Zr_2O_7$ a disordered pyrochlore system, exhibits the spin freezing behavior under the application of the magnetic field. We have performed detailed magnetic studies of $Dy_{2-x}La_xZr_2O_7$ to understand the evolution of the magnetic spin freezing in the system. Our studies suggest the stabilization of the pyrochlore phase with the substitution of non-magnetic La along with the biphasic mixture of fluorite and pyrochlore phases for the intermediate compositions. We observed that the spin freezing ($T_f \sim 17$ K) at higher La compositions ($1.5 \leq x \leq 1.99$) is similar to the field-induced spin freezing for low La compositions ($0 \leq x \leq 0.5$) and the well-known spin ice systems $Dy_2Ti_2O_7$ and $Ho_2Ti_2O_7$. The low-temperature magnetic state for higher La compositions ($1.5 \leq x \leq 1.99$) culminates into a spin-glass like state below 6 K. Cole–Cole plot and Casimir-du Pré fit shows the narrow distribution of spin relaxation time in these compounds.

The geometrical frustration is one of the key aspects of the cubic pyrochlore oxide $A_2B_2O_7$ owing to the distorted spin geometry, and negligible structural disorder[1,2]. In pyrochlore structure, A and B sites form a network of corner-sharing tetrahedra, a quintessential framework for a geometrically frustrated magnet. These materials display a variety of exotic phases like spin ice ($Dy_2Ti_2O_7$ and $Ho_2Ti_2O_7$), spin liquid ($Tb_2Ti_2O_7$), spin glass ($Y_2Mo_2O_7$), order by disorder ($Er_2Ti_2O_7$), Kondo effect ($Pr_2Ir_2O_7$), unconventional anomalous Hall effect ($Nd_2Mo_2O_7$), superconductivity ($Cd_2Re_2O_7$), etc.[3–10].

The magnetic spin ice systems have offered an interesting physics with the signature of magnetic monopole like excitation at low temperature[11–13]. Apart from the spin-ice behavior below ~ 2 K, $Dy_2Ti_2O_7$ also shows a strong frequency dependent spin-freezing at ~ 16 K. However no such feature is seen in the spin-ice $Ho_2Ti_2O_7$ which distinguishes the spin dynamics of $(Ho/Dy)_2Ti_2O_7$[14,15]. Although the $Dy_2Ti_2O_7$ and $Ho_2Ti_2O_7$ systems are extensively studied for spin ice properties, a complete understanding of the phenomenon is still elusive[16,17]. The spin freezing behavior of $Dy_2Ti_2O_7$ is very different from the freezing in spin glasses. Unlike the typical spin glass systems the freezing transition in $Dy_2Ti_2O_7$ enhances with the application of magnetic field and give rise to unusual glassiness[3]. Theoretically, an ideal spin-glass behavior is predicted on the pyrochlore lattice of infinitely large dimensions[18,19]. For the finite dimensional system glass phase is established in the systems that exhibit quenched disorder[2]. However, some of the pyrochlore magnets show spin glass transition, even in the absence of quenched disorder, which is indistinguishable to the typical spin glass systems[20–22].

Among these pyrochlore systems, $Dy_2Zr_2O_7$ (DZO) is quite fascinating, as it shows the emergence of the magnetic field induced spin freezing near 10 K and possess the magnetic entropy of $R[\ln 2 - (1/2)\ln(3/2)]$ in the presence of magnetic field of 5 kOe, which is same as the spin ice $Dy_2Ti_2O_7$[23]. The DZO crystallizes in the disordered pyrochlore phase and does not exhibit any magnetic ordering down to 40 mK[24]. Further partial substitution of Dy by La (up to 15%) stabilizes the pyrochlore phase and spin freezing is observed at a lower magnetic field in comparison to DZO[23].

The stability of the pyrochlore structure and the magnetic rare-earth atom (Dy, Ho, etc.) plays a very important role in determining the low-temperature magnetic spin ice ground state of these systems. In this light, we have studied the structural and magnetic phase diagram of $Dy_{2-x}La_xZr_2O_7$ system. We extend our previous studies of diluted pyrochlore zirconate to a much broader range of dilutions to $0 \leq x \leq 2.0$. In doing so, we observed the evolution of structure from disordered pyrochlore ($0 \leq x \leq 0.5$) to stable pyrochlore phase ($1.5 \leq x \leq 2.0$) through the biphasic mixture of these phases for $0.5 < x < 1.5$. The compounds with disordered pyrochlore

School of Basic Sciences, Indian Institute of Technology Mandi, Mandi, HP 175075, India. ✉email: smoun254@gmail.com

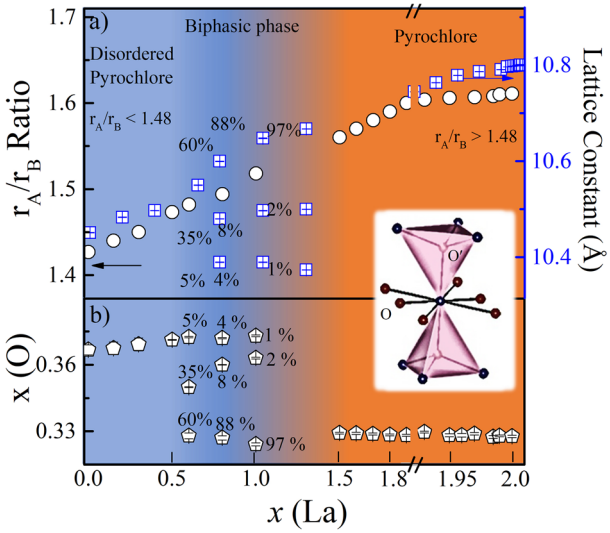

Figure 1. (**a**) Variation in Radius ratio (r_A/r_B) (Left) and lattice constant (Right) as a function of La substitution for $Dy_{2-x}La_xZr_2O_7$; ($0 \leq x \leq 2$). We have extended the scale between $x = 1.9$–2.0 for the better clarity. (**b**) Variation in the position of x(O) parameter of oxygen atom as a function of La concentration. The percentage indicates the contribution from each phase in the refinement.

structures do not show spin freezing in the absence of a magnetic field. In contrast, the stable pyrochlore compounds exhibit $Dy_2Ti_2O_7$ like spin freezing at 17.5 K. The low-temperature phase of $1.5 \leq x \leq 1.99$ compositions show glass-like behavior below 6 K.

Results and discussion

Structural studies. DZO exhibits disordered pyrochlore structure (space group: $Fd\bar{3}\,m$) with the remnants of pyrochlore phase[23–27]. The XRD patterns of $Dy_{2-x}La_xZr_2O_7$ reveal that the compositions corresponding to $0 \leq x \leq 0.5$, adopt disordered fluorite structure. For $0.5 < x < 1.5$, a few super-structure peaks corresponding to pyrochlore structure appear at $2\theta = 14°$ (111), 27° (311), 37° (331), 45° (511), etc. and the main peaks belonging to pyrochlore structure get split. The xrd data in this range was nicely fitted with the biphasic mixture of disordered pyrochlore and clean pyrochlore lattice structures (see supplementary Fig. S3). The Rietveld refinement for $1.5 \leq x \leq 2.0$ confirms the clean face-centered-cubic pyrochlore structure with the observation of super-structure peaks[28,29]. This is also anticipated from the closer value of ionic radius ratio (r_A/r_B) and position of oxygen atom x(O) in the pyrochlore structure (Fig. 1). For a perfect pyrochlore structure the r_A/r_B ranges between 1.48 to 1.78 and ideal value of parameter x(O) ~ 0.3125[30,31]. The deviation from this value, modifies the octahedral (BO_6) and cubic (AO_8) symmetry and results in the change in crytal-field level splitting. For $x \leq 0.5$, the r_A/r_B ratio is less than the expected range of the pyrochlores and the parameter x(O) is close to ~ 0.362 which indicates the formation of disordered fluorite/pyrochlore structure. Here, with $x \geq 1.5$, the r_A/r_B (where r_A = 1.027/1.16 Å for Dy^{3+}/La^{3+} and r_B = 0.72 Å for Zr^{4+}) found to be in the pyrochlore regime (Fig. 1a). The x(O) evolves continuously towards pyrochlore regime with La substitution (Fig. 1b) and supports the stabilization of pyrochlore structure for higher La concentrations. The transformation from disordered pyrochlore to ordered pyrochlore structure along with the positional parameter x(O) would presumably enhanced the crystal field spacing about A site. A systematic shift of peak position towards lower angle on La incorporation indicates the increase of unit cell parameter (see supplementary Fig. S1).

Raman spectra of a pyrochlore structure consist of six Raman active modes; A_{1g}, E_g, and four T_{2g} modes; corresponding to the vibrations of <A-O> and <B-O> bonds[32,33]. The DZO shows no mode (Fig. 2) at 466 cm^{-1} corresponding to the fluorite structure but exhibits the pyrochlore type structural ordering with the presence of weak modes of pyrochlore structure[23,34]. The modes become more intense upon La substitution. The Raman spectra of the biphasic compositions ($0.5 < x < 1.5$) also do not exhibit any extra mode other than the pyrochlore structure and thus indicate the absence of any impurity phase in these compounds. The Raman spectra of $Dy_{2-x}La_xZr_2O_7$ for the compositions $x \geq 1.5$ shows sharper and well pronounced peaks (at 301 cm^{-1} (T_{2g}), 395 cm^{-1} (E_g), 493 cm^{-1} (A_{1g}), 514 cm^{-1} (T_{2g}) and 651 cm^{-1} (T_{2g}) than for $x \leq 0.5$. This is possibly due to the increase in structural symmetry which is consistent with r_A/r_B ratio for La substituted DZO. Additionally, an extra mode at 701 cm^{-1} (marked by M) is observed in all the substituted compounds which was observed around 650 cm^{-1} in the parent compound and attributed to the vibrations of the ZrO_6 octahedra[27,35].

DC magnetization studies. We measured the magnetization of the compounds at a low field (100 Oe) using the zero-field-cooled (ZFC) and field-cooled (FC) protocols. In the previous study[23], we have shown that the compounds having low La composition in $Dy_{2-x}La_xZr_2O_7$; x = 0.0, 0.15, 0.3 exhibit paramagnet-like behavior down to 1.8 K. This behavior sustains up to the La substitution of x = 1.0, but the dc magnetic susceptibility of x = 1.5 shows bifurcation of ZFC and FC curves at T_{irr} ~ 4 K (Fig. 3a). The FC magnetization is completely

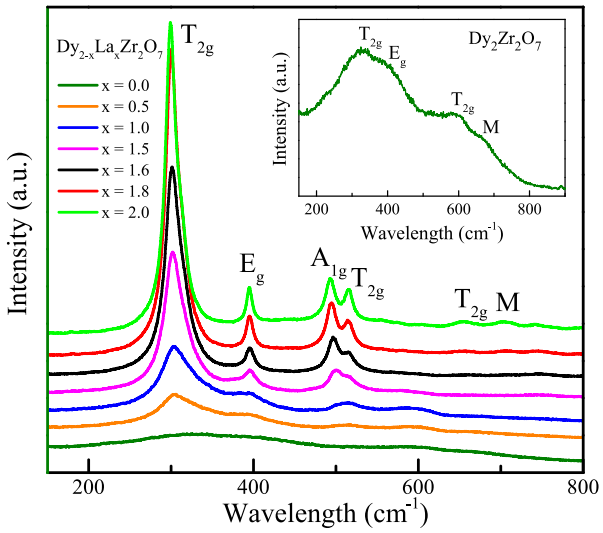

Figure 2. Room temperature Raman spectra of $Dy_{2-x}La_xZr_2O_7$; ($0 \leq x \leq 2$) showing the presence of Raman modes corresponding to pyrochlore structure. Inset: Raman spectra of $Dy_2Zr_2O_7$.

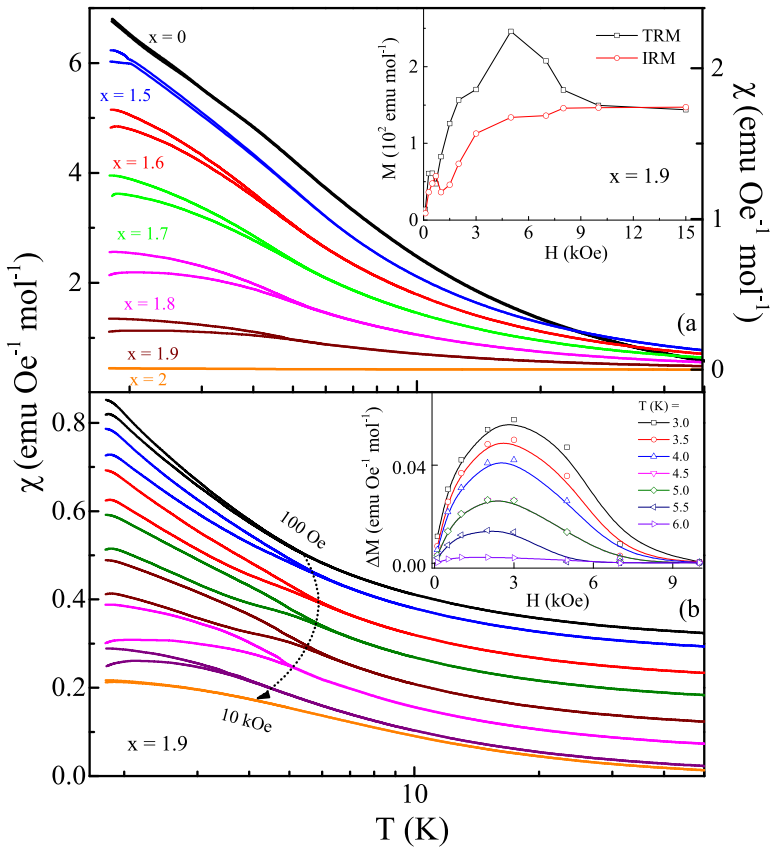

Figure 3. (**a**) Dc magnetic susceptibility χ_{dc} (ZFC and FC) versus T at $H = 100$ Oe for $Dy_{2-x}La_xZr_2O_7$ ($0 \leq x \leq 2$). Inset: Thermo and isothermo remnant magnetization as a function of field at $T = 1.8$ K for $Dy_{0.1}La_{1.9}Zr_2O_7$. (**b**) Dc magnetic susceptibility χ_{dc} (ZFC and FC) versus T at various dc applied field for $Dy_{0.1}La_{1.9}Zr_2O_7$ (data is shifted along y-axis for better visibility of T_{irr}). Inset: Field response of $\Delta M = M_{FC} - M_{ZFC}$ of $Dy_{0.1}La_{1.9}Zr_2O_7$ at various temperature.

reversible, while the ZFC magnetization is irreversible at a fixed magnetic field. The T_{irr} (which is taken at the bifurcation point between the ZFC and FC magnetization) shifts towards higher temperatures for further increase in La concentration (shown in Fig. S6a) and disappeared with the complete replacement of Dy with La ($x = 2.0$). The absence of T_{irr} in the end compound ($La_2Zr_2O_7$: $[Xe]5d^06s^0$) is obvious. The splitting in the ZFC and FC curves can be taken as an indication of the spin-glass phase. In conventional spin-glass systems the glass state is quenched on applying the sufficiently strong field, and the temperature at which the glass state appears decreases on increasing the magnetic field[36]. As shown in Fig. 3b, the bifurcation point T_{irr} slightly increases with the applied field up to 3 kOe and then decreases to low temperature on a further increase of field and disappear at 10 kOe. We have plotted the field response of $\Delta M = M_{FC} - M_{ZFC}$ of $Dy_{0.1}La_{1.9}Zr_2O_7$ at various temperature in the inset of Fig. 3b. It is clearly seen that similar to the field dependence of T_{irr} the difference (ΔM) between the two data sets increases with the applied field up to 3 kOe and no difference between the FC and ZFC magnetization is observed at 10 kOe. Furthermore, the shifting of T_{irr} towards low temperature for $H \geq 3$ kOe and reduction in the absolute value of χ_{dc} under the application of high magnetic field indicates the frozen spin-glass-like state below T_{irr}. Spin glass is a metastable state which arises due to random site distribution and random exchange and leads to a multi-degenerate ground state[2,36,37]. In pyrochlores, glassiness occurs possibly due to the competing interactions, which transform to the glass/frozen state on cooling without any long-range magnetic order. The substitution of non-magnetic La at the magnetic Dy site is bound to affect the magnetic interactions present in the system. The replacement of $3/4^{th}$ of Dy atoms ($x = 1.5$) reduces the overall magnetic interactions, leading to the establishment of spin-glass-like state. This further evident from MH isotherm, where La substitution leads to the 6–8% change in the spin anisotropy in comparison to the $Dy_2Ti_2O_7$ system.

The irreversibility of spin state at low-temperature was further confirmed by examining the isothermal remnant magnetization (IRM) and thermoremnant magnetization (TRM). The IRM and TRM curves shown in the inset of Fig. 3a are consistent with the spin-glass picture[3]. The difference between the magnetization curve below 10 kOe points towards the retained memory of its aged value under the same final condition. This shows that a sufficiently high field can destroy this memory and the behavior is equivalence of ZFC and FC data taken in the same field. Notably, both the magnetization curves merge at a field 10 kOe. Surprisingly, we do not observe any frequency dependence in the ac susceptibility measurement below T_{irr}, which raises some doubt in the magnetic state. Thus, these observations point towards the formation of spin-glass-like state instead of a clean spin glass state. Considering the possibility of long-range cooperative interactions between rare-earth ions, systems often do not get into a clean magnetic state. Some additional local probe measurements are required for a clear understanding. The Curie Weiss fitting of dc susceptibility data (measured at $H = 100$ Oe) in the temperature range 30–300 K shows the dominance of antiferromagnetic interactions in these systems. The obtained parameters are listed in Supplementary Table II.

Figure 4a shows the field response of magnetization at 1.8 K. The magnetization isotherm for DZO (inset of Fig. 4a) increases up to 20 kOe and remains saturated up to the maximum applied field of 70 kOe. The saturation moment (M_s) for DZO (4.8 μ_B/Dy) is close to the $Dy_2Ti_2O_7$ (5 μ_B/Dy) but half of the theoretically expected value (10.64 μ_B/Dy). This indicates strong crystal-field induced anisotropy in the system, which would possibly changed on dilution[38,39]. The substitution of La up to $x \leq 0.3$ exhibits similar behavior as that of DZO[23]. However, for the higher concentration of La ($x \geq 1.5$) magnetization isotherms show a large hysteresis below 7 K and get saturated at the lower field compared to DZO. The obtained values of saturation magnetization for La substituted compounds are nearly half of the free-ion value and vary only 6–8% to the M_s of $Dy_2Ti_2O_7$. These results are in line with crystal field-induced anisotropy in La substituted compounds that do not affect the magnetic moment to a greater extent. The effect of La substitution on anisotropy is measurably small and comparable to the dilution of Dy site with Ca, and quite distinct from the Y substitution[38,40,41].

The irreversibility seen in the dc magnetization (Fig. 3) around 6 K is evident from the magnetic isotherm curve. As shown in Fig. 4b, the magnetic hysteresis for $Dy_{0.1}La_{1.9}Zr_2O_7$ suppressed at 7 K, similar to the dc magnetization where ZFC and FC curves overlap at this temperature. Interestingly, no appreciable hysteresis is found at $H \sim 10$ kOe, at which the bifurcation between the ZFC-FC and IRM-TRM curves is lost.

AC susceptibility studies. The ac susceptibility (χ_{ac}) of $Dy_{2-x}La_xZr_2O_7$ ($0 \leq x < 2$) are shown in Fig. 5, measured to investigate the effect of La substitution on the spin dynamics of the system. The pyrochlore compound $Dy_2Ti_2O_7$ shows the high-temperature spin freezing anomaly at 16 K and spin ice ground state at low-temperature[42]. The replacement of Ti site with isovalent but comparatively larger Zr atom disorder the crystal structure and leads to a very dynamic ground state down to 40 mK[24]. However, the disorder induced by the Zr atom (as discussed by Ramon et al.[24]) is significantly suppressed by applying the magnetic field and shows the re-entrance of $Dy_2Ti_2O_7$ like magnetic state at 10 K with the presence of non-zero residual entropy[23] at 5 kOe. The compounds with La substitution of $x \leq 0.5$ exhibits the paramagnet-like behavior similar to the parent compound in real (χ') and imaginary (χ'') parts of χ_{ac}, measured at zero dc field. Figure 5a,b show the temperature variation of χ' and χ'' for frequency $f = 10$–1000 Hz at zero dc applied field for $DyLaZr_2O_7$ (i.e. $x = 1.0$). As seen, χ_{ac} remains almost featureless up to this concentration, except for the development of weak features near 15 K. This feature develops into a full peak shape anomaly for stable pyrochlore compounds $1.5 \leq x \leq 1.99$ (Fig. 5c). For the biphasic region ($0.5 < x < 1.5$), we observed only a single broad peak which might consist of the peak anomaly from both the ordered phase. The study on the dilution of $Dy_2Ti_2O_7$ by Y and Lu atom by Snyder et al.[40] shows that the evolution of freezing temperature is independent of structural symmetry ($Dy_{2-x}B_xTi_2O_7$: B = Y, Lu form stable pyrochlore structure for all value of x). The effect of Ca^{2+} substitution on the spin freezing in $Dy_2Ti_2O_7$ is similar to the Y^{3+}, however, it suppresses the freezing anomaly to a greater extent[38,42].

The $\chi'(T)$ and $\chi''(T)$ curves show a monotonous rise for all the excitation frequencies with a decrease in temperature (see supplementary Fig. S7). Though the frequency dependence of spin freezing transition indicates the

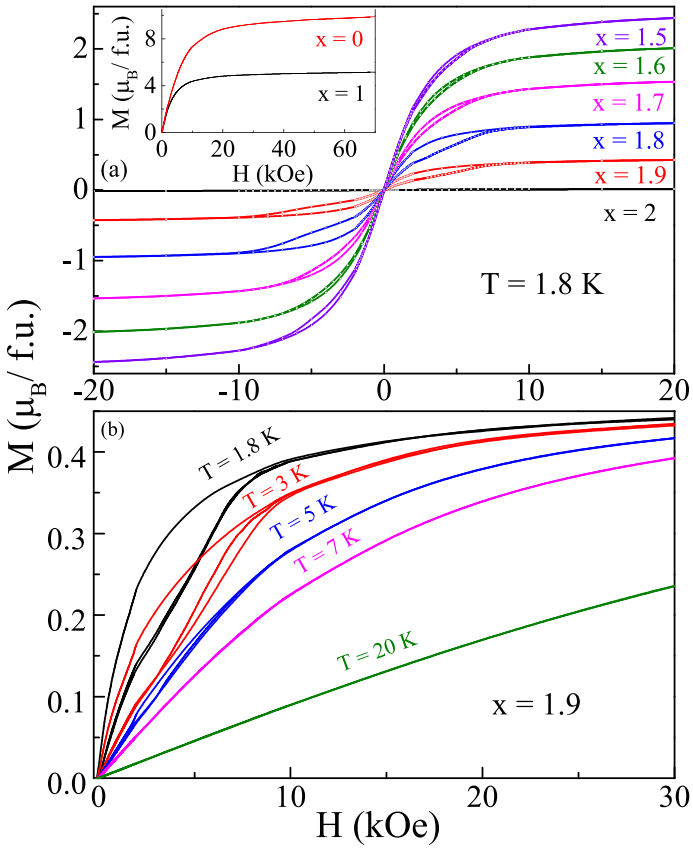

Figure 4. (**a**) Isothermal Magnetization M(H) of $Dy_{2-x}La_xZr_2O_7$; x = 1.5, 1.6, 1.7, 1.8 and 1.9 at 1.8 K. Inset shows the isothermal magnetization at 1.8 K for x = 0, 1. (**b**) Field dependence of magnetization for $Dy_{0.1}La_{1.9}Zr_2O_7$ at T = 1.8, 3, 5, 7 and 20 K.

glassy behavior, the obtained value of Mydosh parameter; $p = \Delta T_f/T_f\,\Delta(\ln f) \sim 0.80$–$0.2$ are much larger than the typical spin-glass value of $p \sim 0.005$–0.01[36], and thus point towards the unusual spin freezing in these systems. Therefore, an alternate explanation is required to understand the spin relaxation in these structurally clean systems. Further the frequency dependence of χ' follows the Arrhenius Law, given by $f = f_o\exp(-E_a/k_BT)$, where E_a is the average activation energy for spin fluctuations (shown in supplementary Fig. S8). The obtained values of the relaxation time (τ) and activation energy E_a are in the range of 10^{-6} sec and 150 (± 20) K respectively. The variations of E_a and τ with La compositions are shown in Fig. 5d, which is of the order of single-ion anisotropy energy and reasonably supports the individual spin flips in these systems. The slow relaxation of spin can be explained based on an increase in energy barrier in the substituted compounds compared to DZO[24]. Further, it is notable that in the stable pyrochlores ($x \geq 1.5$) E_a substantially decreases on increasing the dilution. It is possibly due to the re-entrance symmetry of the pyrochlore structure with La substitution, which effectively changes the magnitude of crystal field spacing associated with the change in lattice constant and electronic structure. Indeed, the X-ray studies indicate that the lattice parameter increases monotonically with La substitution in consistence with the decrease in E_a. The observed behavior is similar to the structural studies on Y and Lu doped $Dy_2Ti_2O_7$ where the rise in E_a correlates with the monotonic decrease in the lattice parameter with dilution[40].

A more striking difference between the observed spin freezing and glassy freezing is found in the frequency distribution of the spin relaxation process. In Fig. 5e, we plot the frequency dependence of normalized χ'' and analysed in term of a Casimir-du Pré relation. This predicts that for a individual spin relaxation time τ, $\chi''(f) = f\,\tau[(\chi_T - \chi_S)/(1 + f^2\tau^2)]$ where χ_T and χ_S are the isothermal and adiabatic susceptibility respectively[38]. We find the close proximity of our data to the theoretical results corresponding to single spin relaxation. The presence of single spin relaxation is also evident from the Cole–Cole plot (see supplementary Fig. S8)[38]. The data points on $\chi''(\chi')$ curves corresponding to different frequencies fall on the semi-circular arc of varying diameters for all compositions. The inset of Fig. 5d shows the variation in α (width of relaxation times) for different compositions. The obtained value of α is quite large from other dense magnetic systems ($DyP_{1-x}V_xO_4$, $Rb_2Cu_{1-x}Co_xF_4$) exhibiting glassy behavior in which the relaxation times are typical of several orders[43,44]. The shape of arc remains unchanged upon La substitution and indicates that the distribution of relaxation times is unaffected and follows the single spin relaxation process for $Dy_{2-x}La_xZr_2O_7$.

We further measured the frequency ($1 \leq f < 1$ kHz) dependence of χ_{ac} to estimate the relaxation time (τ) of the spin freezing (see supplementary Fig. S9). The $\chi''(f)$ shows a well-defined peak above T = 10 K, which shifts with temperature. It is to mention that the evolution of τ for $Dy_2Ti_2O_7$ is linked with the crossover from thermal to

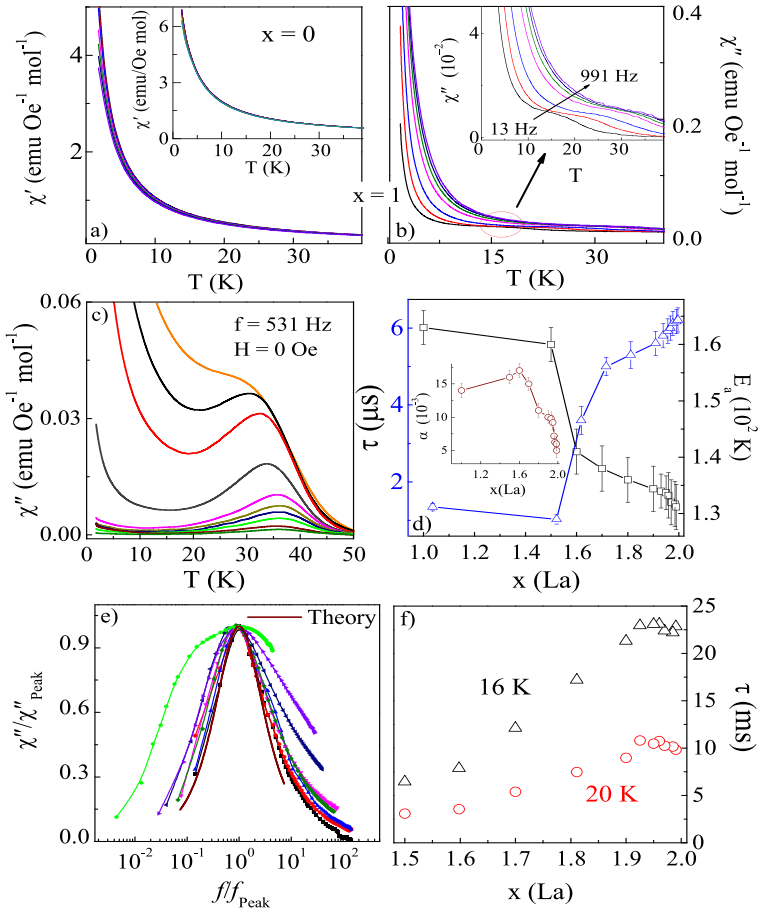

Figure 5. (**a**–**c**) The real χ' and imaginary χ'' parts of ac susceptibility for $Dy_{2-x}La_xZr_2O_7$ ($0 \le x \le 1.99$) measured at $H_{dc} = 0$ Oe for frequencies ranges between $f = 13$–991 Hz. (**d**) Variation of E_a and relaxation time τ for $1 \le x \le 1.99$. Inset shows the variation in Cole–Cole parameter α. (**e**) Casimir-du Pré relation fit for ac susceptibility (**f**) Relaxation time $\tau = 1/2\pi f$ vs x determined from the frequency of χ'' for $1.5 \le x \le 1.99$.

quantum spin relaxation[3,45]. Unlike $Dy_2Ti_2O_7$, the obtained values of τ for $Dy_{2-x}La_xZr_2O_7$ ($x = 1.5$–2.0) follow the Arrhenius behavior. This activated relaxation is responsible for the high-temperature spin freezing observed at $T_f \sim 17.5$ K. These data show that $\tau(x)$ rises monotonically on increasing non-magnetic dilution. It is to note that DZO shows a slower spins relaxation ($\tau = 10^{-1}$ s) at the lowest measuring temperature in comparison to $Dy_2Ti_2O_7$ ($\tau = 10^{-3}$ s)[3]. For $x = 1.0$, no relaxation peak was observed in $\chi''(f)$ plot, but a very weak signal of freezing transition was detected in $\chi''(T)$ plot. In Y and Lu doped $Dy_2Ti_2O_7$[40], the unusual re-entrance of the high-temperature spin-freezing can be understood from the spin relaxation time. The non-monotonic nature of $\tau(x)$ on the La concentration for $Dy_{2-x}La_xZr_2O_7$ is associated with the increase in energy barrier with dilution. Our results for La substitution from 0 to 1.99 showed the disappearance of freezing transition in the disordered pyrochlore phase and its re-emergance on achieving the structural stability in the absence of magnetic field.

Magnetic phase diagram. The magnetic phase diagram of $Dy_{2-x}La_xZr_2O_7$; $x = 0$ - 2.0 has been drawn in Fig. 6. The label T_f and T_{irr} were extracted from the ac and dc magnetic susceptibility. It is clearly seen that the increase in La concentration stabilizes the $Dy_2Ti_2O_7$ like spin freezing transition for $x = 0.5$–1.99. The structurally biphasic region ($0.5 < x < 1.5$) shows only one type of spin freezing only. It quite possible that the spin freezing corresponding to the minor phase get overwhelmed by the spin freezing of majority phase, as the spin freezing transitions of these phases are quite close to each other. For the compositions $x \ge 1.5$, a new spin glass like freezing is observed at low temperatures. The end member of the series $La_2Zr_2O_7$ does not show any sort of the spin freezing.

Conclusions

In conclusion, we have shown that the position of the oxygen atom plays a significant role in determining the crystal structure of $Dy_{2-x}La_xZr_2O_7$ and the pyrochlore phase gets stabilized on La substitution. The low-temperature magnetic ground state of the system evolves from a field-induced spin freezing state for La compositions of $0 \le x \le 0.3$ to the spin freezing in the absence of magnetic filed for $1.5 \le x \le 1.99$. The spin dynamics of the system suggest slower spin relaxation in comparison to $Dy_2Ti_2O_7$. For $1.5 \le x \le 1.99$, the spin freezing is followed by

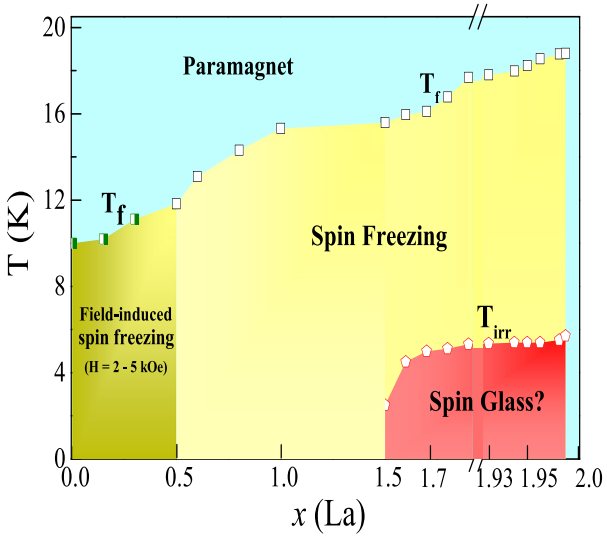

Figure 6. Magnetic phase diagram of $Dy_{2-x}La_xZr_2O_7$; $x = 0–2.0$ showing the evolution of spin freezing transition on La substitution. Data points marked by star are taken from Ref[16] indicating the field induced spin ice phase for $x \leq 0.5$. The compositions between $0.5 < x \leq 1.99$ represents the spin freezing transition (T_f) and the low temperature state culminates to glassy behavior marked by T_{irr}.

a spin glass like state below 6 K. These study suggest the robustness of the spin freezing state in Dy pyrochlore system and may have significant bearing on the observed spin ice behavior in $Dy_2Ti_2O_7$. Our studies would be useful in the understanding of the high temperature spin freezing state in the spin ice systems.

Methods

The polycrystalline compounds of $Dy_{2-x}La_xZr_2O_7$ (x: 0.5, 0.6, 0.8, 1.0, 1.5, 1.6, 1.7, 1.8, 1.9, 2.0) were prepared by the standard solid-state reaction method[23]. The constituent oxides: Dy_2O_3 (Sigma Aldrich, ≥99.99% purity), La_2O_3 (Sigma Aldrich, ≥99.999% purity) and ZrO_2 (Sigma Aldrich, 99% purity) were reacted in the alumina crucible at 1350 °C in ambient atmosphere for 50 hours. The reaction at this temperature was done thrice with the intermediate grindings. The obtained compounds were further pelletized and sintered at 1350 °C for 50 hours. The other compounds $x = 1.93, 1.95, 1.96, 1.97, 1.985, 1.99$ are prepared with solid-state reaction method with slight change in the annealing condition. In the dilution regime ($1.5 \leq x \leq 1.99$) we observed consistency in the structural and magnetic parameter. The spin freezing and irreversibility in dc magnetization is remain prominent even up to the dilution of 99.5%. Magnetic and Heat capacity studies on the $Dy_2Zr_2O_7$ reported by Ramon et al. matches well with our previous studies[24]. Therefore, we believe that the reported results in this manuscript are intrinsic to these system, and are not affected by the preparation conditions. Additionally, we have performed all magnetization measurements on the same piece of sample.

The powder X-ray diffraction measurement on all the compounds was performed using the Rigaku X-ray diffractometer in the 2θ range of 10–90° with the step size of 0.02°. The Rietveld refinement of the X-ray diffraction (XRD) pattern was performed using Fullprof Suite software. Raman spectra of the compound were obtained at 300 K in backscattering geometry by using a Horiba HR-Evolution spectrometer with a 532 nm excitation laser. We study the magnetization as well as the real (χ') and imaginary parts (χ'') of the ac susceptibility (χ_{ac}). The magnetic measurements were performed using Quantum Design built Magnetic Property Measurement System (MPMS) above 1.8 K. In thermoremanent magnetization (TRM) the sample was cooled from 10 K to the desired temperature in the presence of magnetic field, reducing the field to zero at a rate of 0.1 T/min, and then measuring the dc magnetization as a function of time. The isothermal magnetization (IRM) was collected by cooling the sample from 10 K in the absence of a field, then cycling the field from $0 \rightarrow H \rightarrow 0$ and measuring the magnetization as a function of time. The sample was held at H for at least 2 hours to obtain nearly complete relaxation in the field.

Received: 7 July 2021; Accepted: 16 September 2021
Published online: 06 October 2021

References

1. Villain, J. Insulating spin glasses. *Zeitschrift für Physik B Condens. Matter.* **33**, 31–42 (1979).
2. Binder, K. & Young, A. P. Spin glasses: Experimental facts, theoretical concepts, and open questions. *Rev. Mod. Phys.* **58**, 801 (1986).
3. Snyder, J. *et al.* Low-temperature spin freezing in the dy2ti2o7 spin ice. *Phys. Rev. B* **69**, 064414 (2004).
4. Ehlers, G. *et al.* Dynamical crossover in 'hot' spin ice. *J. Phys. Condens. Matter* **15**, L9 (2002).
5. Enjalran, M., Gingras, M. J., Kao, Y., Del Maestro, A. & Molavian, H. The spin liquid state of the tb2ti2o7 pyrochlore antiferromagnet: A puzzling state of affairs. *J. Phys.: Condens. Matter* **16**, S673 (2004).

6. Greedan, J., Sato, M., Yan, X. & Razavi, F. Spin-glass-like behavior in y2mo2o7, a concentrated, crystalline system with negligible apparent disorder. *Solid State Commun.* **59**, 895–897 (1986).
7. Petrenko, O., Lees, M. & Balakrishnan, G. Low-temperature magnetisation process in the cubic pyrochlore quantum antiferromagnet, er2ti2o7. *Eur. Phys. J. B* **86**, 416 (2013).
8. Nakatsuji, S. *et al.* Metallic spin-liquid behavior of the geometrically frustrated kondo lattice pr2ir2o7. *Phys. Rev. Lett.* **96**, 087204 (2006).
9. Taguchi, Y. *et al.* Magnetic field induced sign reversal of the anomalous hall effect in a pyrochlore ferromagnet nd2mo2o7: Evidence for a spin chirality mechanism. *Phys. Rev. Lett.* **90**, 257202 (2003).
10. Jin, R. *et al.* Superconductivity in the correlated pyrochlore cd2re2o7. *Phys. Rev. B* **64**, 180503 (2001).
11. Toews, W. *et al.* Disorder dependence of monopole dynamics in dy2ti2o7 probed via thermal transport measurements. *Phys. Rev. B* **98**, 134446 (2018).
12. Morris, D. J. P. *et al.* Dirac strings and magnetic monopoles in the spin ice dy2ti2o7. *Science* **326**, 411–414 (2009).
13. Jaubert, L. D. & Holdsworth, P. C. Magnetic monopole dynamics in spin ice. *J. Phys.: Condens. Matter* **23**, 164222 (2011).
14. Bramwell, S. *et al.* Spin correlations in ho2ti2o7: A dipolar spin ice system. *Phys. Rev. Lett.* **87**, 047205 (2001).
15. Harris, M. J., Bramwell, S., McMorrow, D., Zeiske, T. & Godfrey, K. Geometrical frustration in the ferromagnetic pyrochlore ho2ti2o7. *Phys. Rev. Lett.* **79**, 2554 (1997).
16. Castelnovo, C., Moessner, R. & Sondhi, S. L. Magnetic monopoles in spin ice. *Nature* **451**, 42–45 (2008).
17. Fennell, T. *et al.* Magnetic coulomb phase in the spin ice ho2ti2o7. *Science* **326**, 415–417 (2009).
18. Kurchan, J., Parisi, G. & Zamponi, F. Exact theory of dense amorphous hard spheres in high dimension i the free energy. *J. Stat. Mech. Theory Exp.* **2**, 10012 (2012).
19. Saunders, T. & Chalker, J. Spin freezing in geometrically frustrated antiferromagnets with weak disorder. *Phys. Rev. Lett.* **98**, 157201 (2007).
20. Taniguchi, T., Munenaka, T. & Sato, H. (IOP Publishing, Spin glass behavior in metallic pyrochlore ruthenate ca2ru2o7. *J. Phys. Conf. Ser.* **145**, 012017 (2009).
21. Gardner, J. *et al.* Glassy statics and dynamics in the chemically ordered pyrochlore antiferromagnet y2mo2o7. *Phys. Rev. Lett.* **83**, 211 (1999).
22. Reimers, J., Greedan, J., Kremer, R., Gmelin, E. & Subramanian, M. Short-range magnetic ordering in the highly frustrated pyrochlore y2mn2o7. *Phys. Rev. B* **43**, 3387 (1991).
23. Sheetal *et al.* Emergence of weak pyrochlore phase and signature of field induced spin ice ground state in dy2-xlaxzr2o7; x= 0, 0.15, 0.3. *J. Phys. Condens. Matter.* **32**, 365804 (2020).
24. Ramon, J. G. A. *et al.* Absence of spin-ice state in the disordered fluorite dy2zr2o7. *Phys. Rev. B* **99**, 214442 (2019).
25. Mandal, B., Garg, N., Sharma, S. M. & Tyagi, A. Preparation, xrd and raman spectroscopic studies on new compounds re2hf2o7 (re= dy, ho, er, tm, lu, y): Pyrochlores or defect-fluorite?. *J. Solid State Chem.* **179**, 1990–1994 (2006).
26. Sayed, F. N. *et al.* Sm2-xdyxzr2o7 pyrochlores: Probing order–disorder dynamics and multifunctionality. *Inorg. Chem.* **50**, 2354–2365 (2011).
27. Glerup, M., Nielsen, O. F. & Poulsen, F. W. The structural transformation from the pyrochlore structure, a2b2o7, to the fluorite structure, ao2, studied by raman spectroscopy and defect chemistry modeling. *J. Solid State Chem.* **160**, 25–32 (2001).
28. Hagiwara, T., Nomura, K. & Kageyama, H. Crystal structure analysis of ln2zr2o7 (ln= eu and la) with a pyrochlore composition by high-temperature powder x-ray diffraction. *J. Ceram. Soc. Jpn.* **125**, 65–70 (2017).
29. Rodriguez-Carvajal, J. Fullprof: a program for rietveld refinement and pattern matching analysis. In *satellite meeting on powder diffraction of the XV congress of the IUCr*, vol. 127 (Toulouse, France:[sn], 1990).
30. Pal, A., Singh, A., Ghosh, A. & Chatterjee, S. High temperature spin-freezing transition in pyrochlore eu2ti2o7: A new observation from ac-susceptibility. *J. Magn. Magn. Mater.* **462**, 1–7 (2018).
31. Kumar, H., Sathe, V. & Pramanik, A. Spin-phonon coupling in hole-doped pyrochlore iridates y2ir1-xrux2o7: A raman scattering study. *J. Magn. Magn. Mater.* **478**, 148–154 (2019).
32. Han, H. *et al.* Electron paramagnetic resonance study of the f-d interaction in pyrochlore iridate gd2ir2o7. *Phil. Mag.* **95**, 3014–3022 (2015).
33. Hasegawa, T. *et al.* Raman scattering study in iridium pyrochlore oxides. In *Journal of Physics: Conference Series*, vol. 200, 012054 (IOP Publishing, 2010).
34. Hozoi, L. *et al.* Longer-range lattice anisotropy strongly competing with spin-orbit interactions in pyrochlore iridates. *Phys. Rev. B* **89**, 115111 (2014).
35. Turner, K. M., Tracy, C. L., Mao, W. L. & Ewing, R. C. Lanthanide stannate pyrochlores (ln2sn2o7; ln= nd, gd, er) at high pressure. *J. Phys.: Condens. Matter* **29**, 504005 (2017).
36. Mydosh, J. *Spin glasses: An experimental introduction, taylor and francis london* (Washington DC, 1993).
37. Huang, C. Some experimental aspects of spin glasses: A review. *J. Magn. Magn. Mater.* **51**, 1–74 (1985).
38. Anand, V., Tennant, D. & Lake, B. Investigations of the effect of nonmagnetic ca substitution for magnetic dy on spin-freezing in dy2ti2o7. *J. Phys.: Condens. Matter* **27**, 436001 (2015).
39. Fukazawa, H., Melko, R., Higashinaka, R., Maeno, Y. & Gingras, M. Magnetic anisotropy of the spin-ice compound dy2ti2o7. *Phys. Rev. B* **65**, 054410 (2002).
40. Snyder, J. *et al.* Quantum and thermal spin relaxation in the diluted spin ice dy2-xmxti2o7 (m= lu, y). *Phys. Rev. B* **70**, 184431 (2004).
41. Lin, T. *et al.* Nonmonotonic residual entropy in diluted spin ice: A comparison between monte carlo simulations of diluted dipolar spin ice models and experimental results. *Phys. Rev. B* **90**, 214433 (2014).
42. Snyder, J., Slusky, J., Cava, R. J. & Schiffer, P. How spin ice freezes. *Nature* **413**, 48 (2001).
43. Dirkmaat, A. *et al.* Frequency dependence of the ac susceptibility in the random anisotropy system dy (p 1–x v x) o 4. *Phys. Rev. B* **36**, 352 (1987).
44. Dekker, C., Arts, A., De Wijn, H., Van Duyneveldt, A. & Mydosh, J. Activated dynamics in a two-dimensional ising spin glass: Rb2cu1-xcoxf4. *Phys. Rev. B* **40**, 11243 (1989).
45. Snyder, J. *et al.* Quantum-classical reentrant relaxation crossover in dy2ti2o7 spin ice. *Phys. Rev. Lett.* **91**, 107201 (2003).

Acknowledgements

We acknowledge the Advanced Material Research Center, IIT Mandi, for the experimental facility. Sheetal is thankful to IIT Mandi and MHRD India for the Senior Research Fellowship.

Author contributions

S. synthesized the samples, performed the experiments. S. and C.S.Y. analyzed the data and wrote the manuscript.

Competing interests

The authors declare no competing interests.

Additional information

Supplementary Information The online version contains supplementary material available at https://doi.org/10.1038/s41598-021-99035-z.

Correspondence and requests for materials should be addressed to S.

Reprints and permissions information is available at www.nature.com/reprints.

Publisher's note Springer Nature remains neutral with regard to jurisdictional claims in published maps and institutional affiliations.